Journal of
Composites Science

MDPI

Article

Overmoulding of Additively Manufactured Titanium Inserts Using Polyoxymethylene (POM)—Evaluation of Bond Quality as a Function of Process Parameters

Teresa Liese [1,*], Julia Richter [2], Thomas Niendorf [2] and Angela Ries [3]

[1] Plastics Technology, Institute of Materials Engineering, University of Kassel, Mönchebergstraße 3, 34125 Kassel, Germany
[2] Metallic Materials, Institute of Materials Engineering, University of Kassel, Mönchebergstraße 3, 34125 Kassel, Germany; julia.richter@uni-kassel.de (J.R.); niendorf@uni-kassel.de (T.N.)
[3] Faculty of Engineering and Mathematics, Bielefeld University of Applied Sciences, Interaktion 1, 33619 Bielefeld, Germany; angela.ries@fh-bielefeld.de
* Correspondence: liese@uni-kassel.de

Abstract: Due to their process-induced porous surfaces, additively manufactured structures are not optimized for applications in which friction is a key factor. To improve the frictional properties of additively manufactured titanium inserts of various thicknesses, two tribologically optimized POM materials, which differ in terms of filler composition and contents, were used to overmould the inserts. The titanium inserts were manufactured in two different building directions, resulting in a variation in surface roughness. The main challenge with respect to overmoulding is to maintain an even, thin plastic layer on the titanium insert. In order to evaluate the adhesion between plastic and metal, the interface is examined by optical microscopy and assessment of the peeling resistance. The peeling test shows that the overmoulded titanium inserts with a higher surface roughness are characterized by a higher peeling resistance. It is further revealed that the POM material with a special filler concept shows superior peeling resistance.

Keywords: hybrid material; mechanical testing; microstructure; injection moulding; 3D-printing

Citation: Liese, T.; Richter, J.; Niendorf, T.; Ries, A. Overmoulding of Additively Manufactured Titanium Inserts Using Polyoxymethylene (POM)—Evaluation of Bond Quality as a Function of Process Parameters. *J. Compos. Sci.* **2021**, *5*, 159. https://doi.org/10.3390/jcs5060159

Academic Editors: Isabel Montealegre-Meléndez, Eva M. Pérez-Soriano and Cristina Arévalo

Received: 7 May 2021
Accepted: 10 June 2021
Published: 15 June 2021

1. Introduction

In recent years, additive manufacturing (AM) has become a mature production technology. The production of near-net shape parts characterized by a high freedom of design are appealing for research and industrial applications [1]. Although all AM processes are based on a layer-wise build-up directly from a CAD model, powder bed fusion (PBF) processes, such as selective laser melting (SLM) and electron beam melting (EBM), are mainly investigated for their ability to produce filigree structures at moderate building rates [2,3]. The latter aspect highlights the main drawback of AM technologies: a tradeoff between granularity and production speed prevails, eventually resulting in relatively high production costs for most AM processes and parts. Therefore, so far only in small-series productions, i.e., in aerospace and medical engineering, these technologies are widely applied. Motivated by those industrial sectors, the nickel-based alloy In718, the stainless steel 316L, and the titanium alloy Ti6Al4V have been in the focus of investigation. In all cases, it has to be considered that, in AM parts, the resulting mechanical properties are often different to conventional manufactured parts [4], so that structural integrity under given loading conditions has to be addressed. On the one hand, process inherent high cooling rates, amongst others, related to small melt pool sizes, are responsible for the change in microstructure. On the other hand, process imperfections, such as pores and a high surface roughness due to several reasons in PBF processing, e.g., lack of fusion, keyholing and melt pool dynamics, result in early failure under cyclic loading [5]. Although these challenges in AM appear in all alloy systems, the effects on the mechanical properties are dependent

on the strength and ductility of the alloy in question [6]. Whereas, for instance, 316L shows a relatively high defect tolerance [7,8] in spite of pores, Ti6Al4V is affected to a great extent by roughness and porosities [9].

Ti6Al4V shows superior performance in many cases, making it the material of choice for many industrial sectors. The high strength at low density, as well as a high corrosion resistance, are appealing for aerospace engineering and automotive industries. Due to its biocompatibility, it is also used as an implant material in medical engineering [10]. In all of these sectors, abrasive behaviour is non-desirable and can result in damage with serious consequences. Therefore, many studies [11–13] have focused on improving the surface quality of additive manufactured parts, since additive manufactured structures without any subsequent treatment are not to be considered ideal friction partners, due to their porous surface. In most studies, the high surface roughness is decreased by subtractive methods as turning and polishing [14–16] in order to enhance the mechanical and tribological behaviour. For conventional manufactured parts, not only subtractive methods but also further approaches such as thin-film coatings, often based on fluoropolymers, e.g., polytetrafluoroethylene (PTFE) [17] and their further modifications [18], are numerously applied and mostly used to improve the frictional properties of metals. These significantly enhance the frictional properties of metallic systems and are firmly established in the field of dry lubrication and as coating layers for bearings and seals. At present, however, there is not sufficient scientific understanding and practical experience, respectively, on the application of polymer coatings to additively manufacture components and their performance. Many coating systems in previous studies aim to improve corrosion resistance and biocompatibility, e.g., hydroxyapatite [19,20] and silver-impregnated coatings [21]. Enrique et al. [22] showed an improved surface quality by electrospark deposition on the surface. Nevertheless, the study revealed a tradeoff between high densities at the surface and a good surface roughness. By coating with metallic materials, the improved surface was mainly accompanied by chemical diffusion and a change in mechanical properties [22,23]. The main challenges in case of polymer-based layers are an even application of the thin layers on the friction surfaces and the establishment of a sufficiently high adhesion, i.e., bond quality, of the layer [24,25]. Obviously, these characteristics are dependent on the additively manufactured structure being characterized by a distinct roughness and the general appearance of the applied material.

In addition to coating, the overmoulding of additively manufactured components is another means of applying a friction-optimized thermoplastic to a metallic surface. Here, the difficulty lies in the adhesion of the two materials. There are several ways of dealing with this issue: the use of an intermediate layer can be considered, using, e.g., thermoplastic elastomers (TPE) [26], as well as the use of a bonding agent between metal and plastic layer [27]. Alternatively, mechanical interlocking can be promoted [28]. In any case, advantageous properties can arise from the overmoulding, i.e., the application of an even and thin plastic layer to the metallic surface.

In this paper, additively manufactured Ti6Al4V inserts of various thicknesses are overmoulded with differently filled polyoxymethylene (POM) materials. POM is used as a classic injection moulding material in gear-wheel applications, as well as in sliding components [29]. As an alternative to PTFE, two different POM materials are used in the present work, which were specifically modified to improve tribological properties. The considered titanium inserts differ in their surface roughness, due to their different building directions. It is shown that the roughness can be used to specifically improve adhesion. Even if the values do not reach the degree of mechanical interlocking that is achieved upon laser texturing [30,31] or by inserting defined micro-structures [32], the building direction and the resulting roughness have a major influence on the bond strength [33]. In order to evaluate the adhesion between plastic and metal, the interface is assessed by optical microscopy and the peeling resistance is studied using peeling tests. In addition to the building direction of the titanium inserts, being related to the resulting roughness, the

influence of the layer thickness of the polymer directly set by the overmoulding process was considered and the final properties were found to be effective.

2. Experimental Methods

2.1. Materials

2.1.1. Additively Manufactured Titanium Inserts

For manufacturing of the titanium inserts, commercial Ti6Al4V powder was used. The powder, which is distributed by Arcam AB (Mölndal, Sweden), is gas atomized with an particle size range of 45 to 100 µm [34,35]. Its nominal chemical composition is provided in Table 1.

Table 1. Nominal chemical specification of powders distributed by Arcam AB [34].

Al	V	C	Fe	O	N	H	Ti
6.0%	4.0%	0.03%	0.1%	0.10%	0.01%	<0.003%	Bal.

The samples were built on supports using an EBM system Arcam A2X (Arcam AB, Mölndal, Sweden). The basic machine settings were set to an accelerating voltage of 60 kV and a current of 15 mA. The beam had a focus offset of 3 mA. The scanning speed was 4530 mm/s with a hatch of 0.1 mm. The powder was deposited with a thickness of 50 µm. Meandering scanning was rotated for every layer by 90°. The EBM process took place under high vacuum at an elevated temperature of about 700 °C.

The additively manufactured titanium inserts were built with two different angles, relative to the building direction (BD), see Figure 1.

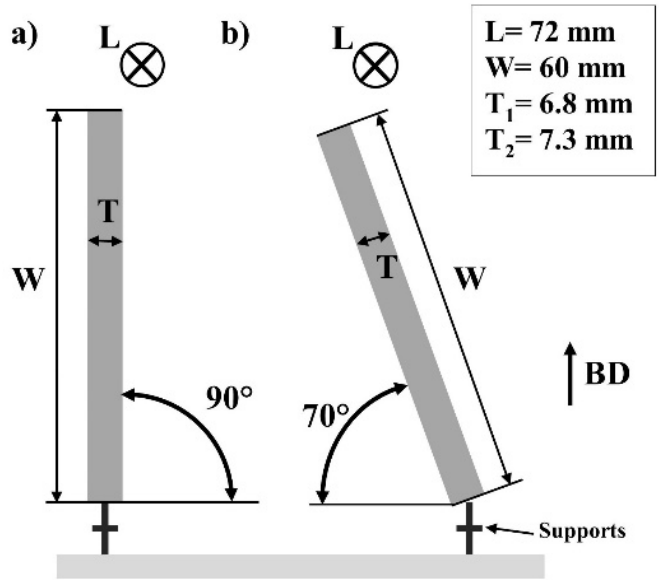

Figure 1. Sample geometry of the titanium inserts with W = width, L = length, T = thickness: (**a**) samples built parallel to the building direction; (**b**) samples built with a tilt angle of 70° with respect to the platform.

The width (W) of the inserts was 60 mm, while samples were 72 mm in length (L). The thicknesses (T) of the samples were set to 6.8 mm and 7.3 mm, respectively. Half of all samples were manufactured perpendicular to the base plate, while the other samples were manufactured at an angle of 70°. The two different tilt angles directly promoted a different roughness on the titanium insert side surfaces [36–39]. Due to the tilt angle of 70°, build-up occurred in a staircase-like manner. Every subsequent discrete layer is built with an offset to the previous one. Therefore, an up-skin and a down-skin evolves. The up-skin shows defined steps, whereas the down-skin is characterized by the melt-induced

infiltration of the sintered powder of the underlying powder bed, eventually forming a non-specific surface roughness.

The surface texture and roughness were determined for each side of the additively manufactured Ti6Al4V inserts based on the profile method, using tactile Surftest SJ-210 (Mitutoyo Corp., Kawasaki, Japan), according to DIN EN ISO 4288:1997. For each of the two different thicknesses of the titanium inserts, three samples were probed. Five individual gauge sections with a length of 0.8 mm each were evaluated.

2.1.2. Thermoplastics Used for Overmoulding

Two different POM types, distributed by Albis Plastic GmbH (Hamburg, Germany), were used for overmoulding the titanium inserts: a POM copolymer with 10 wt.% aramid and 10 wt.% PTFE particles (ALCOM POM 770/1 AR10 PTFE10) and a POM copolymer with less than 5 wt.% special filler for improved sliding friction and wear optimization (ALCOM POM 770/1 SLBV).

To characterize the flow behaviour, the melt flow rate (MFR) was determined according to DIN EN ISO 1133-1:2011 at 220 °C and 230 °C as well as 2.16 kg test load. The melt flow rate indicates the amount of material that flows through a capillary with defined dimensions in 10 min at a specific pressure and temperature. Due to the simplistic measuring principle, reduced shear rates in comparison to normal processing conditions can be assumed. The results are shown in Table 2.

Table 2. MFR at different test temperatures.

Thermoplastic Material	Test Temperature/Test Load			
	220 °C/2.16 kg		230 °C/2.16 kg	
	MFR (g/10 min)	Standard Deviation (g/10 min)	MFR (g/10 min)	Standard Deviation (g/10 min)
POM AR10 PTFE10	7.68	0.0804	10.56	0.1609
POM SLBV	11.93	0.0420	15.24	0.0565

According to the results, type POM AR10 PTFE10 was processed at a higher injection moulding temperature of 230 °C due to the different filling concept, whereas type POM SLBV was processed at 220 °C.

The mechanical properties of both thermoplastic materials were determined by tensile tests, according to DIN EN ISO 527-1:2019 (type 1A) and three-point bending tests, according to DIN EN ISO 178:2017, using a universal testing machine, Zwick Z010 (Zwick Roell, Ulm, Germany). The tests were performed at different test speeds (5 mm/min and 10 mm/min) under displacement control.

2.2. Injection Moulding Process

The titanium inserts were overmoulded with the thermoplastic material on the injection moulding machine Allrounder 320C Golden Edition (Arburg, Lossburg, Germany). The material was dried using the dry air dryer TORO-systems TR-Dry-Jet Easy 15 (GfK Thomas Jakob und Robert Krämer GbR, Igensdorf, Germany) at 110 °C for 2 h before processing. The injection mould is designed for plates with a dimension of 72 × 72 × 10 mm^3 and a film gate with dimensions of 80 × 10.5 × 5.5 mm^3. An aluminium mould with a wall thickness of 0.5 mm was placed into the cavity to prevent damage to the injection mould induced by the titanium inserts, see Figure 2.

It also simplified the handling and positioning of the titanium inserts. The titanium inserts were preheated in an oven at 100 °C to increase the bond strength between the titanium insert and the plastic component, since preheating lowers the surface tension and, thus, improves wetting [40]. Furthermore, by preheating the titanium inserts, the difference between the linear thermal expansion coefficients and the difference between the shrinkage of the plastic and the contraction of the metal is reduced as well. Eventually, this has a

positive effect on the stress state at the interface [40]. After preheating, the titanium insert was placed into the aluminium mould, see Figure 2. The temperatures and parameters chosen for the overmoulding process are listed in Table 3. For the titanium inserts built at an angle of 70°, the surface with the lower roughness (up-skin) was overmoulded.

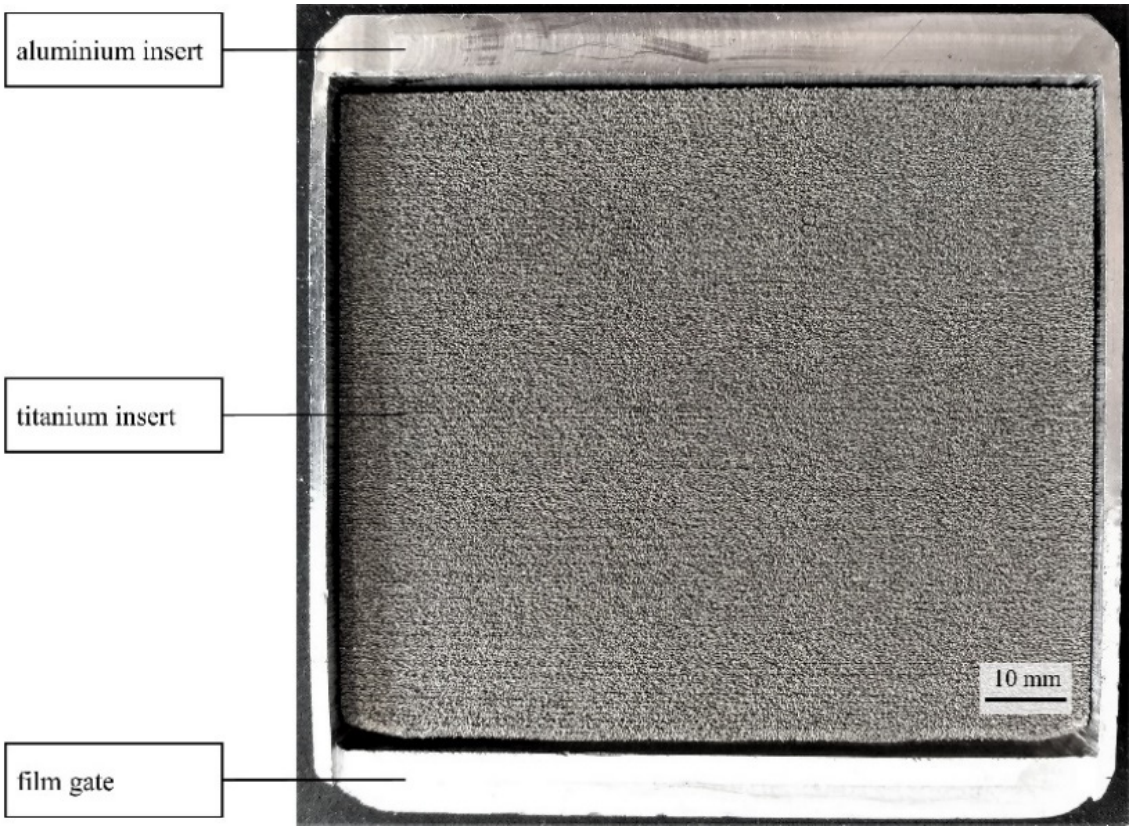

Figure 2. Titanium insert placed within the aluminium mould; the insert was built at an angle of 90°.

Table 3. Parameters used for overmoulding process.

Thermoplastic Material	Mould Temperature	Feeding Section	Zone 1	Zone 2	Zone 3	Zone 4	Zone 5
POM AR10 PTFE10	100 °C	50 °C	210 °C	215 °C	220 °C	225 °C	230 °C
POM SLBV	100 °C	50 °C	200 °C	205 °C	210 °C	215 °C	220 °C
Injection	Phase 1						
	Rate	Pressure					
	(cm^3/s)	(bar)					
	40	900					
Holding	Phase 1			Phase 2			
	Rate	Pressure	Time	Rate	Pressure	Time	
	(cm^3/s)	(bar)	(s)	(cm^3/s)	(bar)	(s)	
	50	700	0.5	50	700	15	

Due to the fact that two different titanium inserts with thicknesses of 7.3 mm and 6.8 mm were overmoulded in a mould with a depth of 10 mm, the overmoulded plastic layers had different thicknesses, i.e., 2.2 mm and 2.7 mm, respectively. When the results

are finally evaluated, the thickness of the overmoulded plastic layer has to be taken into account. The different layer thicknesses are highlighted by the sample notation 2.2 and 2.7.

2.3. Microscopy of the Interface

For microscopy, the interface regions of the overmoulded samples were separated in the middle of the length side, shown in Figure 3, using a universal wet abrasive cut-off machine, Brillant 255 (ATM Qness GmbH, Mammelzen, Germany). The cutting surface was then ground and polished down to 1 µm. For the incident light microscopy, a VHX600 digital microscope from Keyence Deutschland GmbH (Neu-Isenburg, Germany) with a Z100 objective was used. To compare the interfaces, images were always taken at the same magnification.

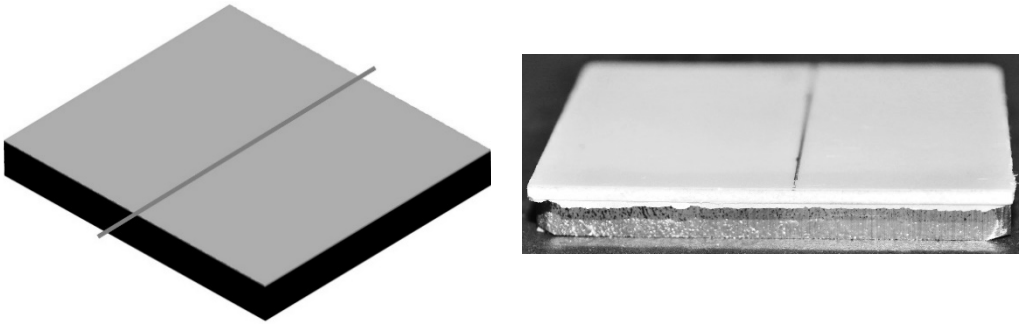

(**a**) (**b**)

Figure 3. (**a**) Section plane considered for incident light microscopy imaging of the interface. (**b**) Overmoulded titanium insert.

2.4. Peeling Test

A test setup based on the VDI guideline 2019:2016 [41] was designed to investigate the peeling resistance of the plastic material on the titanium insert. The VDI guideline 2019:2016 [41] was originally designed for TPE materials to describe the bond strength of TPE and a substrate material. The peeling test was chosen to be able to describe the bond adhesion between two materials by means of investigation of the peel resistance. Other conventional mode I fracture tests, such as ASTM D 5528, instead aim to investigate the resistance of a single material to crack initiation.

In this case, the overmoulded samples were machined using the universal wet abrasive cut-off machine (see Section 2.3) in such a way that the resulting samples had a width of 30 mm and a length of 60 mm. The overmoulded titanium inserts were mounted in the universal testing machine, Z010 (Zwick GmbH & Co. KG, Ulm, Germany), as shown in Figure 4.

The preload was 5 N and the test speed was 5 mm/min. The sample size per batch was n = 3. The protruding tab of the sprue with a width of 7 mm was gripped with a peel-off tool and the plastic layer was removed from the titanium insert. For composites with a rigid and a flexible composite partner, a 90° arrangement is usually selected [42]. For this reason, care was taken during the machining and clamping of the overmoulded samples to ensure that the plastic layer was peeled upwards at an angle of 90°.

For evaluation, the force was determined during the whole test. In addition, the peeling resistance W_P (N/mm) was calculated from the ratio of the maximum force F_M (N) to the sample width b (mm):

$$W_p = F_M/b \quad (1)$$

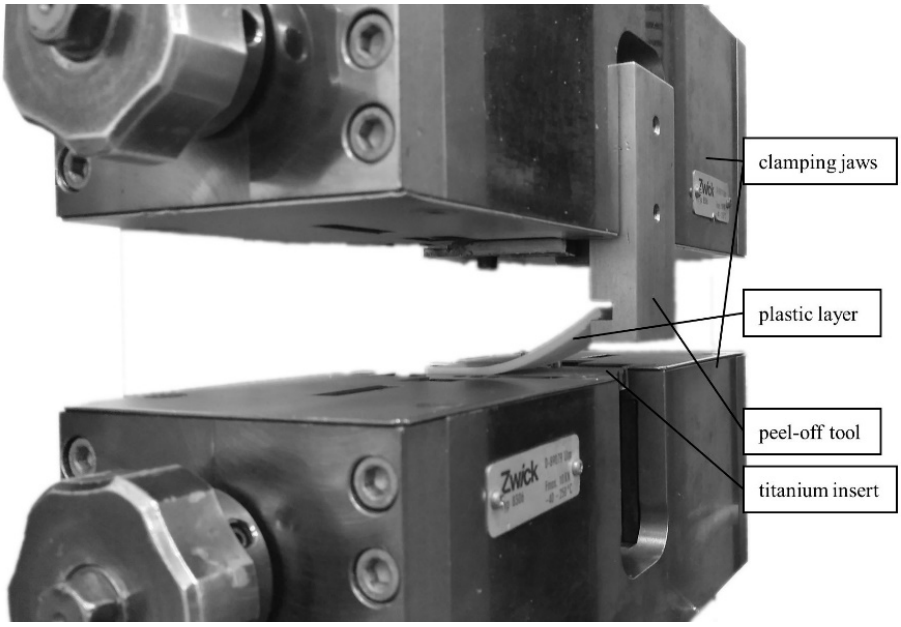

Figure 4. Overmoulded sample mounted in the universal testing machine using custom-built equipment.

3. Results and Discussion

3.1. Characterisation of Relevant Properties of the Base Materials

3.1.1. Roughness of Ti6Al4V

The measurements of surface roughness were conducted in dependence of the building direction. As was already mentioned, surfaces need to be distinguished between side surfaces (parallel to the building direction) and surfaces facing upwards or downwards (henceforth referred to as up-skin and down-skin, respectively). The samples built at an angle of 90°, featuring only side surfaces, revealed an average roughness values of Ra ≈ 30 µm and Rq ≈ 36.9 µm on both sides of the samples. The samples with an inclination angle of 70° are characterized by an up-skin as well as a down-skin surface with different roughnesses. The roughness was measured as Ra ≈ 34.7 µm (Rq ≈ 41.9 µm) in the case of the down-skin surface and Ra ≈ 20.1 µm (Rq ≈ 25.3 µm) for the up-skin surface. Independent of the orientation, the roughness is high in comparison to conventionally manufactured materials. This pronounced roughness is a characteristic and intrinsic process-induced property of AM components. Its actual value is mainly related to the initial powder size, process parameters and building direction. Focusing on the impact of the powder characteristics, the following can be stated: in the case of EBM processing, powder particles with a relatively large size of up to 150 µm are commonly used. Those particles are only partially molten and adhered at the surface, leading to the rough surface. Other powder bed fusion processes, e.g., selective laser melting, employ finer particle sizes, eventually promoting a smoother surface finish [43]. Furthermore, the process of EBM operates at elevated temperatures to sinter the powder before melting. Due to sintering additional powder can adhere to the surface.

Safdar et al. [39] studied the surface roughness of EBM-manufactured parts as a function of parameter and thickness. Upon increase of energy density, either by a change in beam current or scan speed, the roughness of the surface was found to be higher. This correlation was found in several studies, not only for EBM [44], but also for SLM [45]. However, in some studies focusing on SLM built parts, the roughness was reduced by an increase in energy density due to an increase in laser power or a decrease in scan speed [46,47]. Thus, an optimized parameter combination seems to prevail with respect to improved surface quality. Further parameters, such as the hatching distance or focus offset, are quite often not taken into consideration, although a high focus offset was shown to be quite effective to reduce roughness [39,48]. It was further shown that the related process

and part characteristics, e.g., the scan path length imposed by different geometries, can affect the surface quality. In some studies, larger part dimensions resulted in a rougher surface, although manufacturing was conducted using the same parameter settings [39]. In this regard, other studies indicate a contrary correlation [49]. In the present work, no influence on roughness, induced by a change in part dimensions, was found, since the difference in sample thickness was only marginal.

Especially in the case of different building directions, the adherence of the powder particles significantly contributes to final roughness. Since inclined areas need to be built by individual layers with a given layer thickness, the intended shape is approached by a staircase-like structure. The size of the staircase is influenced by the layer thickness and the build angle [50]. At the down-skin of the inclined surface the most pronounced roughness develops [46,51]. In this case, the beam creates a melt pool on the surrounding pre-sintered powder, the latter being characterized by spacing between individual particles. In consequence, the liquid melt flows in those spaces, eventually binding individual particles, finally leading to a high roughness. Due to the low stability of unmolten powder in SLM processing, inclined surfaces are difficult to build with an angle below 45°. The up-skin is characterized by significantly lower roughness in AM processes. The melt pool is created on material that already is solidified, with minimum contact to the surrounding powder. Thus, roughness is mainly caused by individual characteristics of the melt beads. Due to the different parameters used in literature, the roughness differs in most studies. Nevertheless, the average roughness of the EBM-Ti6Al4V material, seen in present work, is in good agreement with other studies reporting on the side surfaces, as well as up-skin and down-skin [49,52]. The average roughness, in the literature, varies between 10 and 40 µm in the case of the side surfaces. Since the present study focuses on the general adhesive properties between titanium and the plastic layer, no further post-process improvement of the surface was considered here. However, several studies show that a change in roughness is possible, most probably allowing for additional adjustments of properties [53].

3.1.2. Mechanical Properties of POM AR10 PTFE10 and POM SLBV

In order to characterize the mechanical properties of the thermoplastic material used, both tensile and bending samples were produced and examined in a tensile test according to DIN EN ISO 527-1:2019 (type 1A), and in a three-point bending test according to DIN EN ISO 178:2017.

The results of the tensile test are given in Table 4, the results of the bending test can be taken from Table 5. The stress–strain diagrams are shown in Figures 5 and 6. Only one exemplary and representative curve per batch is shown in the diagrams.

Table 4. Mechanical properties of the POM copolymers determined in a tensile test, according to DIN EN ISO 527-1 type 1A.

Thermo-Plastic Material	Number of Samples	Test Speed	Mean Value / Standard Deviation	Tensile Modulus	Maximum Stress	Maximum Strain	Stress at Break	Strain at Break
	(–)	(mm/min)		(MPa)	(MPa)	(%)	(MPa)	(%)
POM AR10 PTFE10	$n = 5$	5	x	2571.0	38.9	8.8	38.7	11.4
			s	26.54	0.22	0.34	0.25	1.32
	$n = 5$	10	x	2571.7	39.9	9.0	39.7	12.1
			s	16.28	0.19	0.47	0.20	1.17
POM SLBV	$n = 5$	5	x	2617.4	55.7	9.8	51.5	32.6
			s	16.78	0.18	0.32	1.01	7.65
	$n = 5$	10	x	2623.7	56.5	10.4	52.4	34.9
			s	11.06	0.21	0.29	1.22	7.86

Table 5. Mechanical properties of the POM copolymers determined in a three-point bending test according to DIN EN ISO 178.

Thermo-Plastic Material	Number of Samples	Test Speed	Mean Value / Standard Deviation	Flexural Modulus	Maximum Stress	Maximum Strain	Stress at Break	Strain at Break
	(–)	(mm/min)		(MPa)	(MPa)	(%)	(MPa)	(%)
POM AR10 PTFE10	$n = 5$	5	x	2180.7	65.0	6.7	56.9	11.0
			s	56.27	0.85	0.08	2.05	0.49
	$n = 5$	10	x	2144.7	65.8	6.8	55.3	11.9
			s	41.48	0.62	0.04	1.81	0.49
POM SLBV	$n = 5$	5	x	2188.1	79.9	7.4	70.9	11.4
			s	34.52	0.51	0.07	0.94	0.18
	$n = 5$	10	x	2220.8	81.6	7.5	73.5	11.1
			s	11.62	1.07	0.03	0.96	0.02

The tensile test shows a tensile modulus of 2571 MPa for POM AR10 PTFE10 and 2617 MPa for POM SLBV. The maximum stress is 38.9 MPa for POM AR10 PTFE10 and 55.7 MPa for POM SLBV, while the maximum strain is 8.8% for POM AR10 PTFE10 and 9.8% for POM SLBV. The results at a test speed of 10 mm/min are slightly higher than at 5 mm/min. This can also be deduced from the stress–strain diagram in Figure 5.

As can be seen, the tensile test results show higher tensile modulus, tensile strength, maximum stress, stress and strain at the break for the POM SLBV type, as compared to POM AR10 PTFE10. The results, therefore, contradict the information given in the material data sheet (status from 4 May 2017), where a tensile modulus of 2800 MPa for POM AR10 PTFE10 and 2400 MPa for POM SLBV is stated. The differences seen in the present work to the results from the material data sheet may be due to the processing parameters used, or due to the fact that the composite material becomes more brittle from a filling content of 10% [54].

The three-point bending test revealed a flexural modulus of 2180.7 MPa for POM AR10 PTFE10 and 2188.1 MPa for POM SLBV. The maximum stress is 65 MPa for POM AR10 PTFE10 and 79.9 MPa for POM SLBV, while the maximum strain shows 6.7% for POM AR10 PTFE10 and 7.4% for POM SLBV. The results are, again, slightly higher for a test speed of 10 mm/min; see Figure 6.

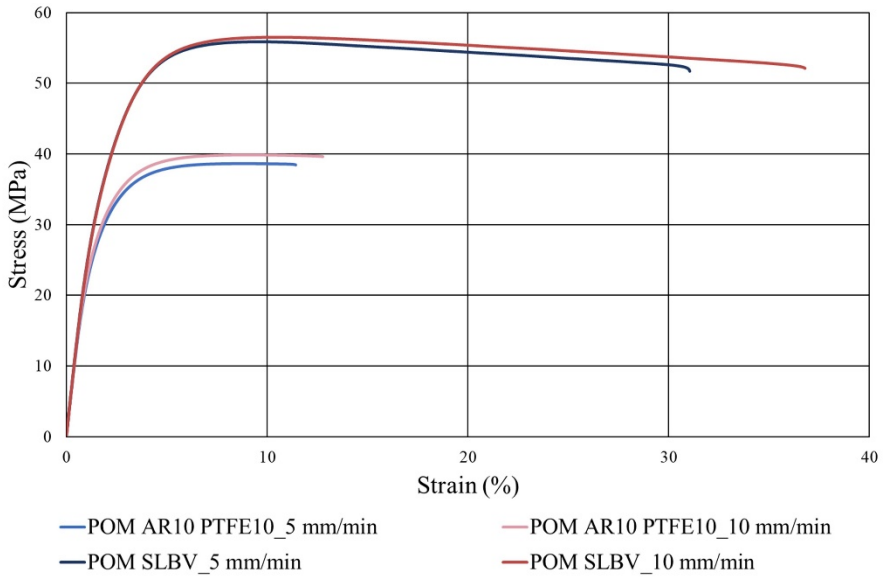

Figure 5. Stress–strain diagram recorded during the tensile test according to DIN EN ISO 527-2 (type 1A), $n = 5$.

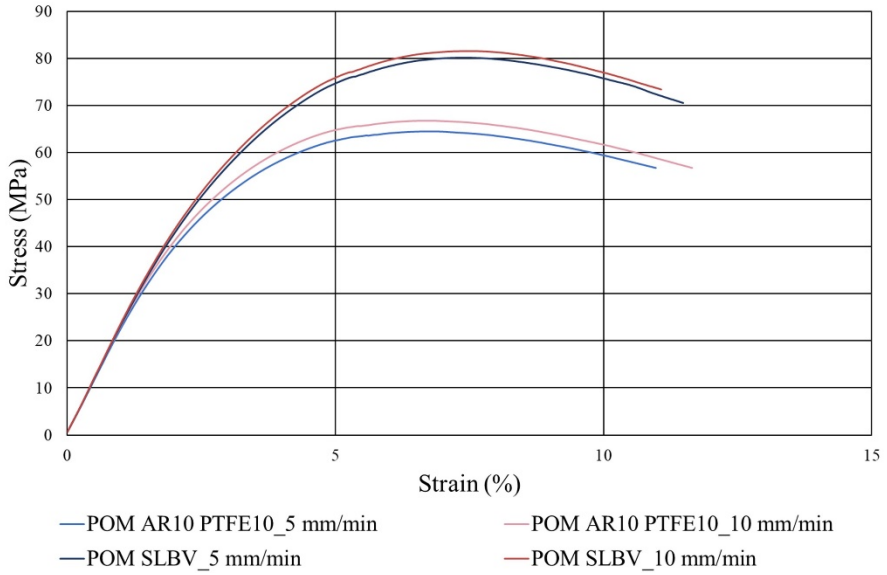

Figure 6. Stress–strain diagram recorded during the three-point bending test according to DIN EN ISO 178, $n = 5$.

3.2. Microscopy of the Interface

In Figures 7 and 8, micrographs of the interfaces of the titanium inserts with POM AR10 PTFE10 and POM SLBV, respectively, are displayed. In both cases, the surfaces of the titanium inserts differ due to the different building directions. Nevertheless, in the case of both building directions (90° and 70°), the penetration of the melt into the rough surface structure is clearly seen.

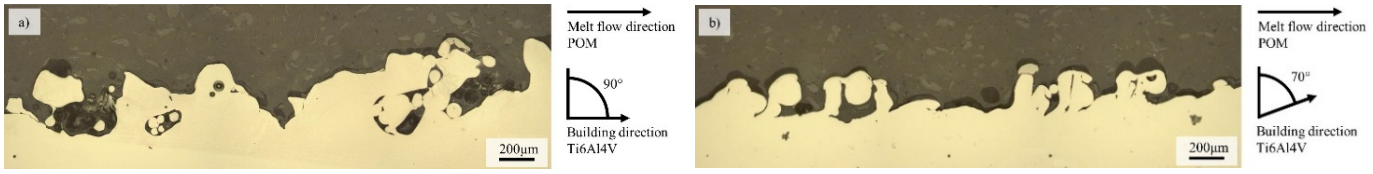

Figure 7. (**a**) Optical micrographs detailing the boundary layer of POM AR10 PTFE10 and the Ti6Al4V insert built at an angle of 90°. (**b**) Optical micrographs detailing the boundary layer of POM AR10 PTFE10 and the Ti6Al4V insert built at an angle of 70°.

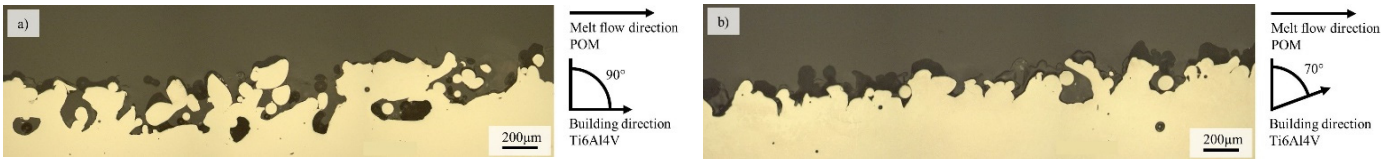

Figure 8. (**a**) Optical micrographs detailing the boundary layer of POM SLBV and the Ti6Al4V insert built at an angle of 90°. (**b**) Optical micrographs detailing the boundary layer of SLBV and the Ti6Al4V insert built at an angle of 70°.

Due to the high weight fraction and the size of the particles in material type POM AR10 PTFE10, the distribution of the particles can be directly determined from the micrographs. The large and bright dots depict the aramid particles, while the small and dark dots are traces of the PTFE particles, compare Figure 7a,b. Obviously, no preferred orientation of the particles can be seen in the images. Thus, no obvious distribution of the particles, directly induced by the melt flow as it is known for glass fibre reinforced composites [54], can be deduced.

Clearly, no particles are apparent in Figure 8. This can be related to the lower filling content and a smaller particle size in material type POM SLBV. An orientation of the particles directly induced by the melt flow direction can, thus, not be revealed in Figure 8.

As can be deduced from the images shown in Figures 7 and 8, the melt does not immediately spread over the entire rough surface of the titanium insert. It is assumed that there are air inclusions between the plastic layer and the titanium insert, which may be due to the fact that the titanium insert has not been sufficiently preheated, so that the local plastic viscosity is lower. Therefore, in many spots, it is more difficult for the thermoplastic material to penetrate the rough surface of the titanium insert [55].

3.3. Peeling Test

The peeling test is intended to provide for a quantitative statement on the adhesive properties between the plastic layer and the titanium insert. For this purpose, Figure 9 summarizes the experimentally determined results, depicting the force-displacement curves of the Ti6Al4V inserts with the overmoulded POM AR10 PTFE10 and with the overmoulded POM SLBV. For the sake of clarity, only one exemplary and representative curve per batch is shown in the diagram.

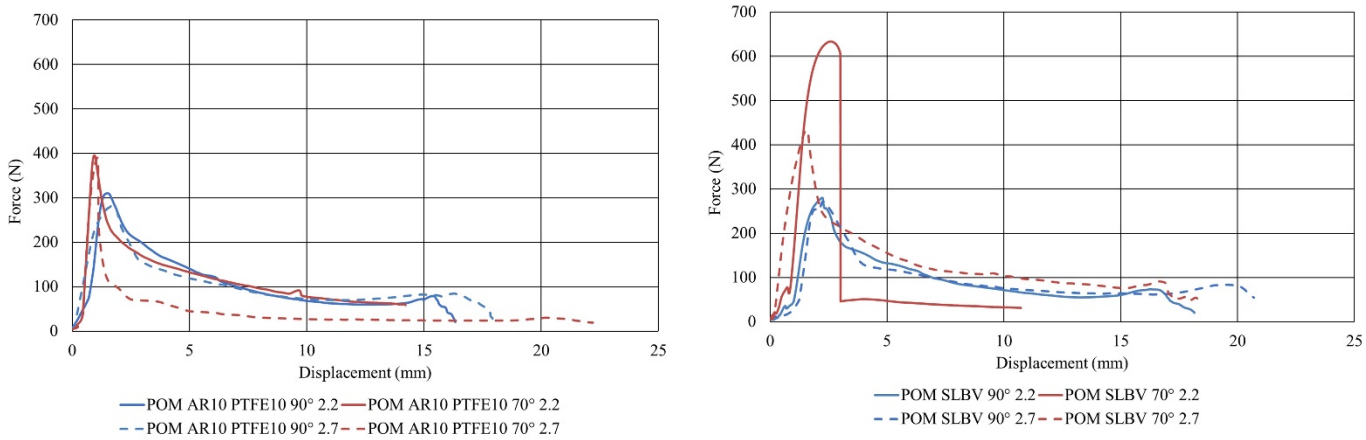

Figure 9. (**a**) Representative force-displacement curves from the peeling tests for different building angles (90° and 70°) and thicknesses (2.2 mm and 2.7 mm) of the plastic layer consisting of POM AR10 PTFE10. (**b**) Representative force-displacement curves from the peeling tests for different building angles (90° and 70°) and thicknesses (2.2 mm and 2.7 mm) of the plastic layer consisting of POM SLBV.

The diagram shows characteristic curves with regard to force-displacement relationships. After a rapid increase in the pull-off force up to a displacement of around 2.7 mm, the pull-off force progressively drops until the plastic layer is either peeled off to a certain point or the plastic layer is fractured with a displacement of around 17 mm to 22.5 mm. As can be seen in Figure 9, the samples in which the Ti6Al4V insert was built at an angle of 70° are characterized by a steeper force increase, regardless of the plastic material used. This can be related to the roughness caused by the tilt angle and the undercuts promoted by this distinct characteristic. The sample made of the material POM SLBV with an angle of 70°, and a plastic layer thickness of 2.2 mm, shows a curve that clearly deviates from the other samples. The strong drop in force at a displacement of about 2.7 mm highlights the tearing off of the plastic layer from the titanium insert. The higher stiffness of the POM SLBV type, in combination with the 70° texturing of the titanium insert, and plastic layer thickness of 2.2 mm, leads to a partial peeling off of the plastic layer. All samples produced from this batch (with a sample size of $n = 3$) show this kind of peeling behaviour.

Figure 10 directly compares the peeling resistances of the different batches in order to provide for an overview of the influence of the layer thickness (derived from the thickness

of the inserts), the processing angle (respectively roughness) and the plastic type (different filling concepts).

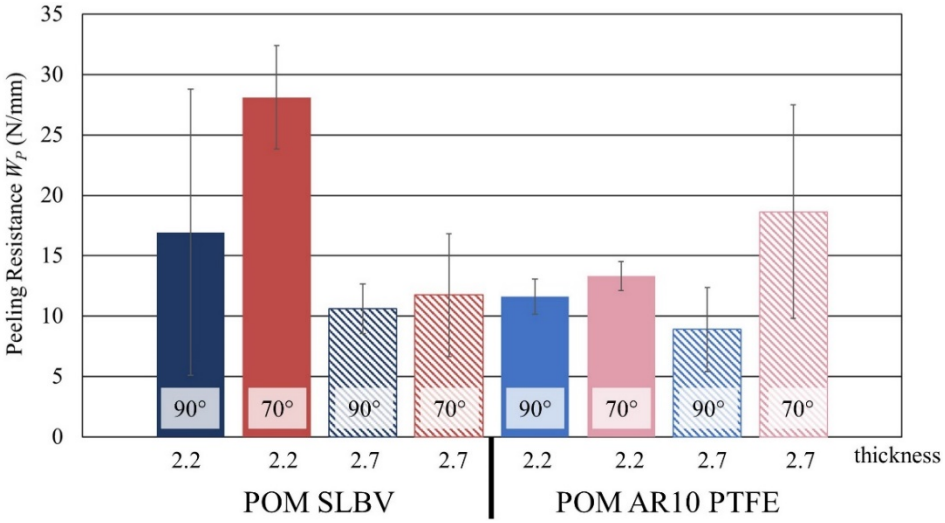

Figure 10. Peeling resistance W_P of the processed samples.

As can be seen in Figure 10, the peeling resistance for material POM AR10 PTFE10 increases for both plastic layer thicknesses, i.e., the rougher the surface of the titanium insert is (from 11.61 (+/−1.44) N/mm to 13.34 (+/−1.20) N/mm for a plastic layer thickness of 2.2 mm and from 8.90 (+/−3.47) N/mm to 18.65 (+/−8.83) N/mm for a plastic layer thickness of 2.7 mm). Similarly, for material POM SLBV, the peeling resistances for both plastic layer thicknesses are higher when the surface of the titanium insert is rougher (from 16.94 (+/−11.84) N/mm to 28.12 (+/−4.29) N/mm for a plastic layer thickness of 2.2 mm and from 10.62 (+/−2.05) N/mm to 11.75 (+/−5.09) N/mm for a plastic layer thickness of 2.7 mm). The POM SLBV samples built at an angle of 90°, with a sample size per batch of $n = 3$, have an outlier that was considered when calculating the standard deviation in Figure 10. If this was excluded from the calculation, this material combination would show an even lower peeling resistance than for samples built at an angle of 70°. For this reason, the outlier was considered in the calculation of the standard deviation, as the results are consistent with the findings in the literature.

Basically, the following three observations can be made: it can be stated that material type POM SLBV with a lower particle content and smaller particle sizes as well as a different filling concept, especially with a plastic layer thickness of 2.2 mm, has a higher peeling resistance than material type POM AR10 PTFE10, contrary to expectations. It was assumed that a higher filling content leads to a stronger interfacial bond strength, since additional force is required to break the polymer and particles [33]. In the samples presented here, 10 wt.% PTFE particles are added in addition to 10 wt.% aramid fibres, which is why the anti-adhesion properties are particularly distinctive, eventually leading to a lower interfacial bond strength.

Furthermore, the samples built at an angle of 70° have a higher peeling resistance and adhesive strength to those built at an angle of 90°. This can be attributed to the building direction of the samples, as shown in Figure 1. An increased roughness is obviously beneficial for the adhesive behaviour.

In addition, the samples produced with a thickness of 6.8 mm are characterized by an inferior peeling resistance, as compared to the 7.3 mm thick samples. This could be attributed to the resulting layer thickness of the 2.7 mm plastic instead of the 2.2 mm plastic for the titanium inserts manufactured with a thickness of 7.3 mm.

In most cases, the plastic layer did not peel off completely. Residues of Ti6Al4V powder were found on the plastic layer. No distinction could be made between the different batches

in terms of the proportion of remaining Ti6Al4V powder residues. Adhesive failure can therefore be assumed in all cases.

4. Conclusions

Process-related challenges of the present test series were the even application of thin, polymer-based layers on the friction surfaces of additively manufactured titanium substrates and the promotion of a superior adhesion of the layer. Key factors are obviously the most relevant characteristics of the additively manufactured structure, which show a certain roughness, and the applied POM material, the latter being studied with different filling concepts. The following conclusions can be drawn from the results obtained so far:

Different layer thicknesses of the plastic material can be realized. Care must be taken to ensure that the titanium insert fits exactly into the aluminium insert, otherwise the complete titanium insert will be overmoulded instead of solely the friction surface. To intently set a higher roughness of the titanium inserts, these can be built at lower inclination angles, e.g., in present work at an angle of 70°.

The peeling tests revealed that both the surface roughness of the titanium inserts and the different filling concepts of the POM material affect the final peeling resistance. The samples built at an angle of 70° have a higher peeling resistance and adhesive strength than those built at an angle of 90°. Furthermore, the POM material with a lower particle content and a different filling concept showed a higher peeling resistance in the peeling test.

Author Contributions: Conceptualization, T.L. and A.R.; methodology, T.L. and J.R.; validation, T.L. and J.R.; formal analysis, T.L. and J.R.; investigation, T.L. and J.R.; resources, T.L. and J.R.; data curation, T.L. and J.R.; writing—original draft preparation, T.L. and J.R.; writing—review and editing, T.L., J.R., T.N. and A.R.; visualization, T.L. and J.R.; supervision, T.N. and A.R.; project administration, T.N. and A.R.; funding acquisition, T.N. All authors have read and agreed to the published version of the manuscript.

Funding: T.N. acknowledges financial support by AiF/IGF (Contract # 19689 BG/2).

Institutional Review Board Statement: Not applicable.

Informed Consent Statement: Not applicable.

Data Availability Statement: The raw/processed data required to reproduce these findings cannot be shared at this time as the data also form part of an ongoing study.

Acknowledgments: The authors would like to thank the company Albis Plastic GmbH for providing the thermoplastic materials for this investigation.

Conflicts of Interest: The authors declare no conflict of interest. The funders had no role in the design of the study; in the collection, analysis, or interpretation of data; in the writing of the manuscript, or in the decision to publish the results.

References

1. DebRoy, T.; Wei, H.L.; Zuback, J.S.; Mukherjee, T.; Elmer, J.W.; Milewski, J.O.; Beese, A.M.; Wilson-Heid, A.; De, A.; Zhang, W. Additive manufacturing of metallic components—Process, structure and properties. *Prog. Mater. Sci.* **2018**, *92*, 112–224. [CrossRef]
2. Brenne, F.; Niendorf, T.; Maier, H.J. Additively manufactured cellular structures: Impact of microstructure and local strains on the monotonic and cyclic behavior under uniaxial and bending load. *J. Mater. Process. Technol.* **2013**, *213*, 1558–1564. [CrossRef]
3. Niendorf, T.; Brenne, F.; Schaper, M. Lattice Structures Manufactured by SLM: On the Effect of Geometrical Dimensions on Microstructure Evolution during Processing. *Metall. Mater. Trans. B* **2014**, *45*, 1181–1185. [CrossRef]
4. Brenne, F.; Leuders, S.; Niendorf, T. On the Impact of Additive Manufacturing on Microstructural and Mechanical Properties of Stainless Steel and Ni-base Alloy. *BHM* **2017**, *162*, 199–202. [CrossRef]
5. Gunther, J.; Krewerth, D.; Lippmann, T.; Leuders, S.; Troster, T.; Weidner, A.; Biermann, H.; Niendorf, T. Fatigue life of additively manufactured Ti-6Al-4V in the very high cycle fatigue regime. *Int. J. Fatigue* **2017**, *94*, 236–245. [CrossRef]
6. Droste, M.; Gunther, J.; Kotzem, D.; Walther, F.; Niendorf, T.; Biermann, H. Cyclic deformation behavior of a damage tolerant CrMnNi TRIP steel produced by electron beam melting. *Int. J. Fatigue* **2018**, *114*, 262–271. [CrossRef]
7. Riemer, A.; Leuders, S.; Thone, M.; Richard, H.A.; Troster, T.; Niendorf, T. On the fatigue crack growth behavior in 316L stainless steel manufactured by selective laser melting. *Eng. Fract. Mech.* **2014**, *120*, 15–25. [CrossRef]

8. Brenne, F.; Niendorf, T. Damage tolerant design by microstructural gradation—Influence of processing parameters and build orientation on crack growth within additively processed 316L. *Mater. Sci. Eng. A* **2019**, *764*, 138186. [CrossRef]
9. Gunther, J.; Leuders, S.; Koppa, P.; Troster, T.; Henkel, S.; Biermann, H.; Niendorf, T. On the effect of internal channels and surface roughness on the high-cycle fatigue performance of Ti-6Al-4V processed by SLM. *Mater. Des.* **2018**, *143*, 1–11. [CrossRef]
10. Hitzler, L.; Merkel, M.; Hall, W.; Ochsner, A. A Review of Metal Fabricated with Laser- and Powder-Bed Based Additive Manufacturing Techniques: Process, Nomenclature, Materials, Achievable Properties, and its Utilization in the Medical Sector. *Adv. Eng. Mater.* **2018**, *20*, 1700658. [CrossRef]
11. Denti, L.; Bassoli, E.; Gatto, A.; Santecchia, E.; Mengucci, P. Fatigue life and microstructure of additive manufactured Ti6Al4V after different finishing processes. *Mater. Sci. Eng. A* **2019**, *755*, 1–9. [CrossRef]
12. Koch, C.; Richter, J.; Vollmer, M.; Kahlmeyer, M.; Niendorf, T.; Böhm, S. Adhesively bonded joints in components manufactured via selective laser melting. *Proc. Inst. Mech. Eng. C J. Mech. Eng. Sci.* **2020**, *235*, 518–526. [CrossRef]
13. Maleki, E.; Bagherifard, S.; Bandini, M.; Guagliano, M. Surface post-treatments for metal additive manufacturing: Progress, challenges, and opportunities. *Addit. Manuf.* **2021**, *37*, 101619. [CrossRef]
14. Breidenstein, B.; Brenne, F.; Wu, L.; Niendorf, T.; Denkena, B. Effect of Post-Process Machining on Surface Properties of Additively Manufactured H13 Tool Steel. *HTM J. Heat Treatm. Mater.* **2018**, *73*, 173–186. [CrossRef]
15. Brandao, A.D.; Gumpinger, J.; Gschweitl, M.; Seyfert, C.; Hofbauer, P.; Ghidini, T. Fatigue Properties of Additively Manufactured AlSi10Mg-Surface Treatment Effect. *FDMD* **2017**, *7*, 58–66. [CrossRef]
16. Kaynak, Y.; Kitay, O. The effect of post-processing operations on surface characteristics of 316L stainless steel produced by selective laser melting. *Addit. Manuf.* **2019**, *26*, 84–93. [CrossRef]
17. Harris, K.L.; Pitenis, A.A.; Angela, A.; Sawyer, W.G.; Krick, B.A.; Blackman, G.S.; Kasprzak, D.J.; Junk, C.P. PTFE Tribology and the Role of Mechanochemistry in the Development of Protective Surface Films. *Macromulecules* **2015**, *40*, 3739–3745. [CrossRef]
18. Lim, W.S.; Khadem, M.; Anle, Y.; Kim, D.E. Fabrication of polytetrafluoroethylene-carbon nanotube composite coatings for friction and wear reduction. *Polym. Compos.* **2018**, *39*, E710–E722. [CrossRef]
19. Yan, C.; Hao, L.; Hussein, A.; Wei, Q.; Shi, Y. Microstructural and surface modifications and hydroxyapatite coating of Ti-6Al-4V triply periodic minimal surface lattices fabricated by selective laser melting. *Mater. Sci. Eng. C* **2017**, *75*, 1515–1524. [CrossRef]
20. Kokubo, T. Formation of biologically active bone-like apatite on metals and polymers by a biomimetic process. *Thermochim. Acta* **1996**, *280*, 479–490. [CrossRef]
21. Croes, M.; Bakhshandeh, S.; van Hengel, I.A.J.; Lietaert, K.; van Kessel, K.P.M.; Pouran, B.; van der Wal, B.C.H.; Vogely, H.C.; Van Hecke, W.; Fluit, A.C.; et al. Antibacterial and immunogenic behavior of silver coatings on additively manufactured porous titanium. *Acta Biomater.* **2018**, *81*, 315–327. [CrossRef]
22. Enrique, P.D.; Marzbanrad, E.; Mahmoodkhani, Y.; Jiao, Z.; Toyserkani, E.; Zhou, N.Y. Surface modification of binder-jet additive manufactured Inconel 625 via electrospark deposition. *Surf. Coat. Technol.* **2019**, *362*, 141–149. [CrossRef]
23. Yang, X.; Zhang, J.; Sagar, S.; Dube, T.; Kim, B.-G.; Jung, Y.-G.; Koo, D.D.; Jones, A.; Zhang, J. Molecular dynamics modeling of mechanical and tribological properties of additively manufactured AlCoCrFe high entropy alloy coating on aluminum substrate. *Mater. Chem. Phys.* **2021**, *263*, 124341. [CrossRef]
24. Fielden-Stewart, Z.; Coope, T.; Bacheva, D.; Kim, B.C. Effect of the surface morphology of SLM printed aluminium on the interfacial fracture toughness of metal-composite hybrid joints. *Int. J. Adhes. Adhes.* **2021**, *105*, 102779. [CrossRef]
25. Hertle, S.; Kleffel, T.; Worz, A.; Drummer, D. Production of polymer-metal hybrids using extrusion-based additive manufacturing and electrochemically treated aluminum. *Addit. Manuf.* **2020**, *33*, 101135. [CrossRef]
26. Drummer, D.; Schmachtenberg, E.; Hülder, G.; Meister, S. MK^2—A novel assembly injection molding process for the combination of functional metal surfaces with polymer structures. *J. Mater. Process. Technol.* **2010**, *210*, 1852–1857. [CrossRef]
27. Schuberth, A.; Göring, M.; Lindner, T.; Töberling, G.; Puschmann, M.; Riedel, F.; Scharf, I.; Schreiter, K.; Spange, S.; Lampke, T. Effect of new adhesion promoter and mechanical interlocking on bonding strength in metal-polymer composites. *IOP Conf. Ser. Mater. Sci. Eng.* **2016**, *11*, 012041. [CrossRef]
28. Thoppul, S.D.; Finegan, J.; Gibson, R.F. Mechanics of mechanically fastened joints in polymer-matrix composite structures—A review. *Compos. Sci. Technol.* **2009**, *69*, 301–329. [CrossRef]
29. Kaiser, W. *Kunststoffchemie für Ingenieure. Von der Synthese bis zur Anwendung*, 5th ed.; Carl Hanser: Munich, Germany, 2021.
30. Gebauer, J.; Fischer, M.; Lasagni, A.F.; Kuhnert, I.; Klotzbach, A. Laser structured surfaces for metal-plastic hybrid joined by injection molding. *J. Laser Appl.* **2018**, *30*, 032021. [CrossRef]
31. Bergmann, J.P.; Stambke, M. Potential of laser-manufacturd polymer-metal hybrid joints. *Phys. Procedia* **2012**, *39*, 84–91. [CrossRef]
32. Kleffel, T.; Drummer, D. Investigating the suitability of roughness parameters to assess the bond strength of polymer-metal hybrid structures with mechanical adhesion. *Compos. B Eng.* **2017**, *117*, 20–25. [CrossRef]
33. Lucchetta, G.; Marinello, F.; Bariani, P.F. Aluminum sheet surface roughness correlation with adhesion in polymer metal hybrid overmolding. *CIRP Ann.* **2011**, *60*, 559–562. [CrossRef]
34. Arcam EMB. Arcam Titanium Ti6AL4V ELI. Available online: http://www.arcam.com/wp-content/uploads/Arcam-Ti6Al4V-ELI-Titanium-Alloy.pdf (accessed on 18 October 2018).
35. Lu, S.L.; Qian, M.; Tang, H.P.; Yan, M.; Wang, J.; StJohn, D.H. Massive transformation in Ti-6Al-4V additively manufactured by selective electron beam melting. *Acta Mater.* **2016**, *104*, 303–311. [CrossRef]

36. Sidambe, A.T. Three-dimensional surface topography characterization of the electron beam melted Ti6Al4V. *Met. Powder Rep.* **2017**, *72*, 200–205. [CrossRef]
37. Weißmann, V.; Drescher, P.; Seitz, H.; Hansmann, H.; Bader, R.; Seyfarth, A.; Klinder, A.; Jonitz-Heincke, A. Effects of Build Orientation on Surface Morphology and Bone Cell Activity of Additively Manufactured Ti6Al4V Specimens. *Materials* **2018**, *11*, 915. [CrossRef]
38. Wang, P.; Sin, W.J.; Nai, M.L.S.; Wei, J. Effects of Processing Parameters on Surface Roughness of Additive Manufactured Ti-6Al-4V via Electron Beam Melting. *Materials* **2017**, *10*, 1121. [CrossRef]
39. Safdar, A.; He, H.Z.; Wei, L.Y.; Snis, A.; de Paz, L.E.C. Effect of process parameters settings and thickness on surface roughness of EBM produced Ti-6Al-4V. *Rapid Prototyp. J.* **2012**, *18*, 401–408. [CrossRef]
40. Li, X.; Liu, F.; Gong, N.; Huang, P.; Yang, C. Enhancing the joining strength of injection-molded polymer-metal hybrids by rapid heating and cooling. *J. Mater. Process. Technol.* **2017**, *249*, 386–393. [CrossRef]
41. VDI-Fachbereich Kunststofftechnik. VDI-Fachbereich Kunststofftechnik. VDI 2019 Testing the adhesion of thermoplastic elastomers (TPE) on substrates. In *VDI Manual Plastics Technology*; VDI Society Materials Engineering, Ed.; Beuth: Berlin, Germany, 2016; p. 15.
42. Ehrenstein, G.W.; Kopczynska, A.; Caseri, W.; Schirle, M.; Hennemann, O.-D. Kleben. In *Handbuch Kunststoff-Verbindungstechnik*; Ehrenstein, G.W., Ed.; Carl Hanser: Munich, Germany, 2004; pp. 426–516.
43. Rafi, H.K.; Karthik, N.V.; Gong, H.J.; Starr, T.L.; Stucker, B.E. Microstructures and Mechanical Properties of Ti6Al4V Parts Fabricated by Selective Laser Melting and Electron Beam Melting. *J. Mater. Eng. Perform.* **2013**, *22*, 3872–3883. [CrossRef]
44. Ge, W.; Han, S.; Fang, Y.C.; Cheon, J.; Na, S.J. Mechanism of surface morphology in electron beam melting of Ti6Al4V based on computational flow patterns. *Appl. Surf. Sci.* **2017**, *419*, 150–158. [CrossRef]
45. Majeed, A.; Ahmed, A.; Salam, A.; Sheikh, M.Z. Surface quality improvement by parameters analysis, optimization and heat treatment of AlSi10Mg parts manufactured by SLM additive manufacturing. *Int. J. Lightweight Mater. Manuf.* **2019**, *2*, 288–295. [CrossRef]
46. Koutiri, I.; Pessard, E.; Peyre, P.; Amlou, O.; De Terris, T. Influence of SLM process parameters on the surface finish, porosity rate and fatigue behavior of as-built Inconel 625 parts. *J. Mater. Process. Technol.* **2018**, *255*, 536–546. [CrossRef]
47. Dursun, G.; Ibekwe, S.; Li, G.Q.; Mensah, P.; Joshi, G.; Jerro, D. Influence of laser processing parameters on the surface characteristics of 316L stainless steel manufactured by selective laser melting. *Mater. Today* **2020**, *26*, 387–393. [CrossRef]
48. Rashid, R.A.R.; Ali, H.; Palanisamy, S.; Masood, S.H. Effect of process parameters on the surface characteristics of AlSi12 samples made via Selective Laser Melting. *Mater. Today* **2017**, *4*, 8724–8730. [CrossRef]
49. Razavi, S.M.J.; Van Hooreweder, B.; Berto, F. Effect of build thickness and geometry on quasi-static and fatigue behavior of Ti-6Al-4V produced by Electron Beam Melting. *Addit. Manuf.* **2020**, *36*, 101426. [CrossRef]
50. Strano, G.; Hao, L.; Everson, R.M.; Evans, K.E. Surface roughness analysis, modelling and prediction in selective laser melting. *J. Mater. Process. Technol.* **2013**, *213*, 589–597. [CrossRef]
51. Kranz, J.; Herzog, D.; Emmelmann, C. Design guidelines for laser additive manufacturing of lightweight structures in TiAl6V4. *J. Laser Appl.* **2015**, *27*, S14001. [CrossRef]
52. Rubino, F.; Scherillo, F.; Franchitti, S.; Squillace, A.; Astarita, A.; Carlone, P. Microstructure and surface analysis of friction stir processed Ti-6Al-4V plates manufactured by electron beam melting. *J. Manuf. Process.* **2019**, *37*, 392–401. [CrossRef]
53. Spitaels, L.; Ducobu, F.; Demarbaix, A.; Rivière-Lorphèvre, E.; Dehombreux, P. Influence of Conventional Machining on Chemical Finishing of Ti6Al4V Electron Beam Melting Parts. *Procedia Manuf.* **2020**, *47*, 1036–1042. [CrossRef]
54. Osswald, T.A.; Menges, G. *Materials Science of Polymers for Engineers*, 3rd ed.; Carl Hanser: Munich, Germany, 2012.
55. Ramani, K.; Moriarty, B. Thermoplastic Bonding to Metals via Injection Molding for Macro-Composite Manufacture. *Polym. Eng. Sci.* **1998**, *38*, 870–877. [CrossRef]